Progress toward using ICF to measure light-ion nuclear cross sections

Mark Yuly, Stephen Padalino, Micah Christensen, Joshua Bowman.

I. Introduction and Motivation

The measurement of low energy cross sections for light ion nuclear reactions represents a nearly unexplored frontier in nuclear physics. Most of these cross sections have never been directly measured at relevant thermonuclear energies, despite the fact that stellar and big bang nucleosynthesis models require as input accurate measurements of these cross sections.

The reason is, unfortunately, these reactions are extremely difficult to measure using standard accelerator techniques because of the very small cross sections at the energies involved, typically only a few keV. For this reason, these nucleosynthesis models typically rely on cross sections extrapolated from measurements at higher energies using S-factor or other techniques. This may lead to large uncertainties in the predictions of these models or even result in incorrect predictions [1].

For reasonable beam currents and targets, to obtain good statistics in an accelerator experiment would take decades or even centuries of beam time even for the most probable reactions. On the other hand, because inertial confinement fusion (ICF) is a thermonuclear process involving a macroscopic amount of nuclear fuel, the number of interacting ions is so large that a measurable number of product nuclei could be obtained in less than 1 ns. As shown in Table 1, cross sections obtained by S-factor extrapolations [2] and predicted by the code TALYS-1.9 [3] were used to calculate expected ICF yields using the OMEGA laser for a large number of low energy deuteron and triton reactions expected to have the largest cross sections, that is, (d,p), (t,p), (t,γ) and (t,α). These reactions on light nuclei typically result in products that beta decay with a half-life between 20 ms and 10 s. The reactions highlighted in orange in Table 1 are the best candidates for measurement using the OMEGA laser at the Laboratory for Laser Energetics (LLE), with an estimated 10^5 to 10^7 product nuclei produced per shot. The green highlighted reactions would become feasible if the yield could be increased by 100-1000 times, such as at the National Ignition Facility (NIF).

The proposed measurement technique is to capture and count the decays of the radioactive product nuclei produced during the implosion. DT or tritium-filled capsules could be doped with an appropriate fraction of the desired reactant isotope (in Table 1 a fraction of 1% was assumed). During the implosion, the desired nuclear reactions would occur producing the product nuclei of interest, which would be dispersed in the expanding plasma but unable to escape before the plasma thermalized and recombined to form a neutral gas. A sample of this gas will be collected and trapped, allowing the beta decays of the product nuclei to be detected and counted. From the measured decay curve, the number of trapped product nuclei would be obtained, which would allow the reactivity for the original thermonuclear reaction to be determined, assuming the efficiencies of the trap and detector can be established. This technique would avoid many of the difficulties usually associated with ICF experiments, which typically directly measure the radiation produced during the implosion. This very intense prompt radiation pulse overwhelms traditional nuclear detectors, making it impossible to identify particles on an event-by-event basis. By capturing then counting the decay of the reaction products, the measurement can be made in the much quieter environment milliseconds or even seconds after the shot. Individual beta decays could then be detected and identified event by event, and the energy of each beta particle individually measured.

Table 1. Product half-life, reactant natural abundances, and predicted yields for a number of light ion reactions that may be studied using ICF. The predicted yields are based on two typical OMEGA shots. For the estimates shown, in each case the target capsule was assumed to be doped with 1% of the appropriate reactant isotope. For the (d,p) reactions, the 50-50 DT OMEGA shot 39794 was used, which had a 2.8 μm thick SiO_2 capsule filled with 20 atm of deuterium-tritium mix that reached an ion temperature of 11.8 keV. For the (t,p), (t,γ) and (t,α) reactions OMEGA shot 77951 was used, a tritium-filled SiO_2 capsule "exploding pusher" that reached 18.3 keV. No cross sections have been previously measured or calculated at any energy for ^{3}H(t,γ)^{6}He, so the predicted yield is based on assuming a branching ratio of 10^{-7}, which is simply an estimated "best case". For other reactions, reactivities were calculated using S-factor extrapolations [4] and TALYS-1.9 [5]. For ^{11}B(d,p)^{12}B [6] and ^{15}N(d,p)^{16}N [7] for which data are available at higher energies, TALYS underpredicts the cross sections by as much as a factor of 100.

Reaction	Product Half-life	Reactant Abundance	Predicted Yield
^{3}H(t,γ)^{6}He	807 ms	^{3}H fill	8×10^{4}
^{6}Li(t,p)^{8}Li	840 ms	7.6%	$0.2\text{-}1\times10^{7}$
^{7}Li(t,α)^{6}He	807 ms	92.4%	$0.7\text{-}2\times10^{6}$
^{9}Be(t,α)^{8}Li	840 ms	100%	5×10^{5}
^{9}Be(t,γ)^{12}B	20.2 ms	100%	18
^{10}B(t,p)^{12}B	20.2 ms	19.9%	5770
^{11}B(d,p)^{12}B	20.2 ms	80.1%	534
^{13}C(t,γ)^{16}N	7.1 s	1.1%	1
^{13}C(t,α)^{12}B	20.2 ms	1.1%	677
^{13}C(t,p)^{15}C	2.45 s	1.1%	111
^{14}N(t,p)^{16}N	7.1 s	99.6%	16
^{15}N(d,p)^{16}N	7.1 s	0.4%	0.15

Three possible ways to collect the product nuclei are being considered, as shown in Figure 1.

1. **Turbomolecular pump trap.** A fraction of the gas atoms leaving the target enter a long tube placed as closely as possible to the target center. Assuming the gas is relatively inert and does not stick to the tube or surfaces in the chamber, it would only take a few milliseconds for the gas atoms to bounce down the tube and enter the turbopump, which would compress them into the phoswich detector attached to the output port. The phoswich detector consists of an 84 mm x 84 mm x 246 mm outside dimensions by 18 mm thick hollow rectangular box made of EJ-240 plastic scintillator, which has a long 285 ns decay time. Lining the box is a 1 mm thick layer of EJ-212 scintillator, having decay constant 2.4 ns. Beta particles from radioactive nuclei which decay inside the detector box can be identified by their dE-E signature and counted. This trap and detector were constructed in 2019 (see Figure 13), the initial results are described later in this report.

2. **Ion pump trap.** Similar to the turbopump trap, gas would enter the ion pump through a long tube. In this case, however, the gas would be re-ionized inside the triode ion pump, then accelerated toward a cathode plate where it would be neutralized and scattered toward the pump wall where it would implant. If the steel pump wall is replaced by a foil backed by the phoswich detector, it would be possible to detect the beta decays of the ions implanted in

the foil. In this case, the thin fast and thick slow plastic scintillators would form the wall between the ion pump magnet and the pump.

3. **Getter trap.** In this technique, atoms coming from the target strike a getter film located as close as possible to the target chamber center. The getter film would be a thin layer or foil of a material known to react chemically with the atoms containing the desired product nuclei. Behind the getter, a 10 mm diameter phoswich detector using the scintillation materials described previously would identify and count beta particles from decays occurring in the getter. One possibility to be explored is using external electric fields to cause inert gas atoms to implant into the getter. This trap and detector is being assembled this summer (2020) and is currently being tested (see Figure 13).

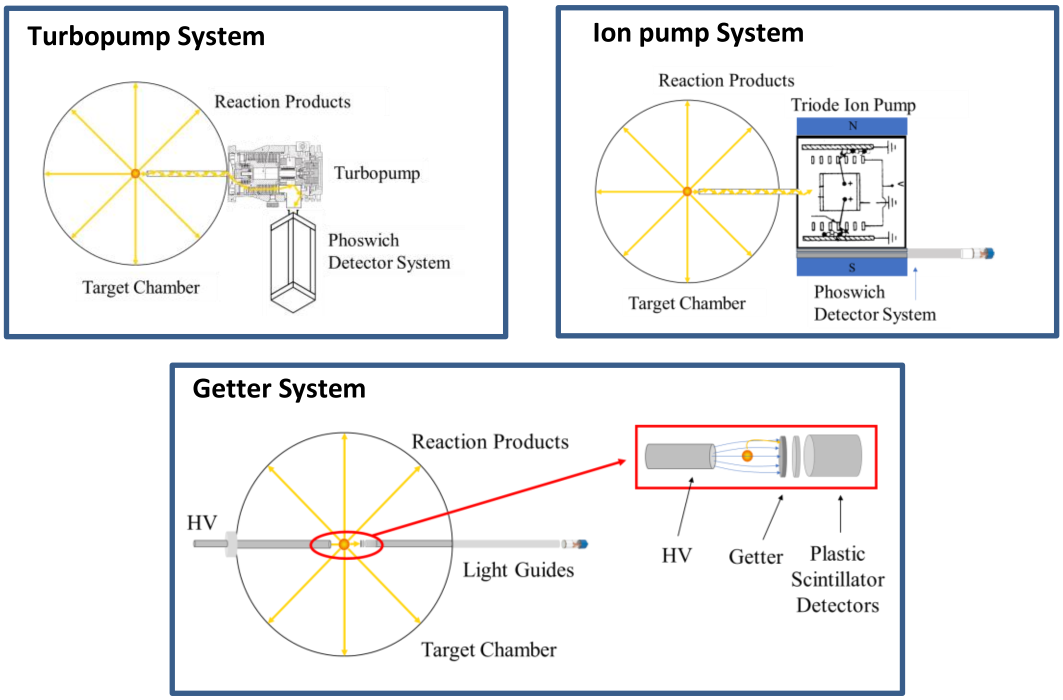

Figure 1. Techniques for capturing product nuclei. In the turbopump trap **(upper left)** the neutral gas containing the product nuclei enters a long tube that directs it into a turbopump. The output port leads the gas to a hollow rectangular phoswich detector where the gas is trapped and product nuclei decays are counted. The ion pump trap **(upper right)** works in a similar fashion, except when the gas reaches the triode ion pump the atoms are re-ionized and an electric field causes them to implant in the pump wall. Decays of implanted product nuclei will be counted using a thin phoswich detector between the pump wall and ion pump magnet. In the getter trap **(lower center)** the atoms containing product nuclei chemically bind to the getter material, and the decays are counted by a small phoswich detector behind the getter. One idea is to use an electric field to cause inert atoms to implant into the getter.

To date, several milestones have already been passed in this project, the details of which are described in the indicated references below.

1. During the summer of 2016 the ability to create ^{6}He via the ^{9}Be(n,α)^{6}He reaction was demonstrated using the SUNY Geneseo Pelletron accelerator. The ^{6}He beta decays were detected and the short 807 ms half-life was measured using a silicon dE-E detector telescope [8].

2. In summer 2017 a small phoswich detector was built similar to the proposed "getter" detector, but without the long light guide or getter material. This detector was tested using the ^{9}Be(n,α)^{6}He reaction and was also able to detect the ^{6}He and measure its half-life [9].

3. A test vacuum chamber was assembled and used for initial tests of the turbopump trap during the summer of 2018. Radioactive ^{41}Ar, which beta decays with a half-life of 109 minutes, was made at SUNY Geneseo using the $^{40}Ar(d,p)^{41}Ar$ reaction and brought to Houghton College where it was injected as a quick pulse into the test chamber. The gas was subsequently captured by the turbopump trap. A silicon detector and a high purity germanium detector, both presenting only a very small solid angle, were used to count beta particles and gamma rays, respectively, coming from the sealed turbopump foreline [10].

4. A hollow phoswich turbopump trap detector subtending solid angle of almost 4π was constructed during the summer of 2019 to capture the gas that was collected by the turbopump trap [11]. This detector was tested at the very end of the summer so the results will be presented in this report.

5. A ride along test was carried out during a series of high-yield OMEGA DT shots on Dec. 17, 2019 for the purpose of testing both the "getter trap" type detector from (2) and the turbopump trap detector from (4) above. The results of these tests will also be presented in this report.

II. Remaining Questions

While many of the requirements needed to develop this technique into a viable measurement system have been met, there are several key questions that still remain to be answered.

Q1. Can a measurable amount of the product material be collected?

a) How do we know what fraction of the product nuclei were collected?
b) How do we know what fraction of the collected nuclei were detected?

Q1 is being addressed in three ways. First, attempts to calculate the expected yield for the nuclear reactions in Table 1 are ongoing, particularly for the $^3H(t,\gamma)^6He$ reaction for which no previous measurements or theoretical predictions have been made. In particular, an attempt is being made to use the code AZURE2 [12] to calculate this cross section. AZURE2 uses the R-matrix formalism to describe different reactions in the same compound system simultaneously with a single set of parameters. This will allow other reactions that pass through the ^6He compound nucleus to be used in the fit of the parameters needed to calculate the $^3H(t,\gamma)^6He$ cross section. This is made difficult, however, by the very limited number of previous measurements that have been made for reactions having ^6He as the compound nucleus, but similar calculations for $^3H(t,t)^3H$ [13] and $^3H(t,2n)^4He$ [13, 14, 15] may be useful here.

In addition, the Geant4 simulation of the detectors, described in Section V, may be used to calculate the absolute efficiency of the detectors, providing the answer to Q1 (b)., with the caveat that this requires understanding the energy calibration of the thick and thin scintillators.

Finally, the planned "exploding wire" experiments, described in Section VI, will hopefully answer Q1 (a), by allowing a known activity of a radioactive material to be produced using the accelerator, and then quickly vaporized and released isotopically into the vacuum chamber. This material will then be trapped and the decays counted, allowing the fraction of the total number collected to be determined.

Q2. Is the "low" background rate after the shot low enough?

a) What is the background rate?
b) What is the composition of the background radiation?
c) What and where are the sources of background radiation?
d) How does background depend on time?

e) Can good beta decay events be identified and selected electronically?

f) Can background be reduced using shielding?

To answer these questions, an OMEGA ride-along experiment was carried out in which detectors were placed near the target chamber for several high yield shots, as described in Section IV. Q2 (a) and (d). can be answered directly, while the others can be approached by comparing the test results to Geant4 detector simulations, allowing shielding and electronics to be fine-tuned. A future ride-along experiment will be needed to test these improvements.

III. Test of the Turbopump Trap using $^{40}Ar(d,p)^{41}Ar$ (July 2020)

The 2019 report [11] introduced an experiment that was then underway to test the hollow rectangular turbopump trap; the results will be described here. In this experiment, the $^{40}Ar(d,p)^{41}Ar$ reaction was used to produce ^{41}Ar, which beta decays with a 109 min half-life and has a beta endpoint energy of 1.2 MeV.

A PVC gas cell was attached to the end of the 15R beamline on the SUNY Geneseo Pelletron, where it was filled with argon at atmospheric pressure as shown in Figure 2. When filling with argon both valves were opened and the end cap was removed to flush out as much air as much as possible. Then the rear PVC valve and the fill line valve were closed and the first PVC valve left open. The total volume of the gas cell is approximately 200 mL, and the sealed volume between the two valves is about 80 mL.

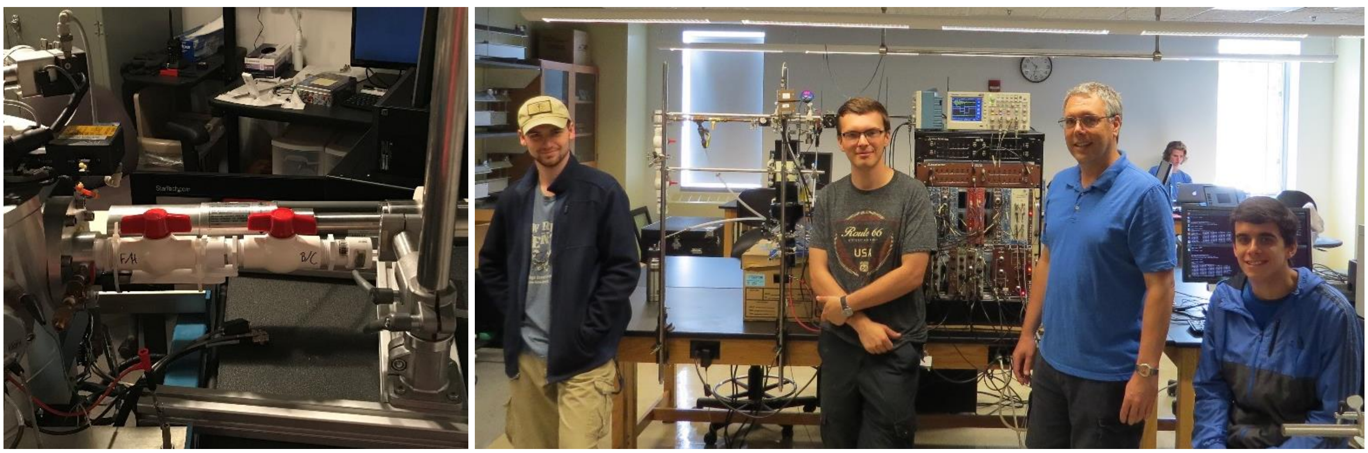

Figure 2. $^{40}Ar(d,p)^{41}Ar$ Test. (Left) A gas cell containing ^{40}Ar was attached to the end of the beamline on the SUNY Geneseo pelletron. Deuterons striking the ^{40}Ar created ^{41}Ar. **(Right)** Houghton students Steven Raymond, Tyler Kowalewski and Sonny Ferri transported the gas cell, now containing a mixture of ^{40}Ar and ^{41}Ar, to the detector station where they introduced the gas mixture into the previously evacuated turbopump trap detector and counted the ^{41}Ar beta decays.

The ^{40}Ar gas was irradiated for 2 hours with an approximately 4 nA beam of 2 MeV deuterons that entered the cell through a thin Kapton window, in which deuterons lost about 270 keV. At the end of 2 hours, the gas cell was removed from the beamline and brought to the evacuated detector, where it was attached to the detector manifold. Argon trapped in the top portion of the cell, above the first red valve, was pumped out, then the detector and gas cell were valved off from the forepump and the final red valve was opened allowing the $^{40}Ar/^{41}Ar$ mixture to flow into the detector. Counting began approximately 5 minutes after the beam was stopped.

Using the technique described in the 2019 report [11] to integrate over the energy loss of the deuterons in the gas yields a range of about 40 mm for the approximately 1.7 MeV deuterons exiting the Kapton window. Along this path, the number of $^{40}Ar(d,p)^{41}Ar$ reactions can be integrated, assuming the cross section follows the R-matrix fit described in Ref. [11], yielding approximately 3.5 million ^{41}Ar nuclei produced. Of this number, only about 40% would be trapped in the central portion of the gas cell. Then, when the gas was allowed to fill the detector, which has an inner volume of about 484 mL, only about 80% would end up in the detector, or about 1.1 million ^{41}Ar nuclei. In this estimate the volume of the connecting tubes and valves and decays during the transit time were neglected.

Figure 3 shows the 2D particle identification histograms obtained in the experiment. In order to determine the region of the 2D histogram that corresponds to beta decay events, a ^{207}Bi source, which decays by beta emission and also releases monoenergetic electrons of about 0.5 and 1 MeV, was inserted into the detector. Events inside the green quadrilateral were considered to be electrons and counted in order to create the growth curve. A fit to the grown curve, shown in the final panel of Figure 3, yielded $(5 \pm 0.1) \times 10^5$ nuclei, or about 50% of the predicted total number. Given the large number of assumptions made in estimating the number of ^{41}Ar nuclei produced in the gas cell, this value for the absolute detector efficiency should not be taken too seriously, but it is nevertheless encouragingly large. In making this estimate, it was assumed that all beta decay events were selected by the green quadrilateral cut on the 2D histogram in Figure 3. This is obviously not true, and, as is illustrated in Figure 10, probably rejected most of the lower energy part of the beta spectrum which has an endpoint of only 1.2 MeV. Clearly, once the energy scale is set, the Geant4 simulation could be used to more accurately set the cut on beta decay events. This should allow us to reach even higher absolute efficiencies than 50%, which is already much better than was obtained using the silicon detector in 2018.

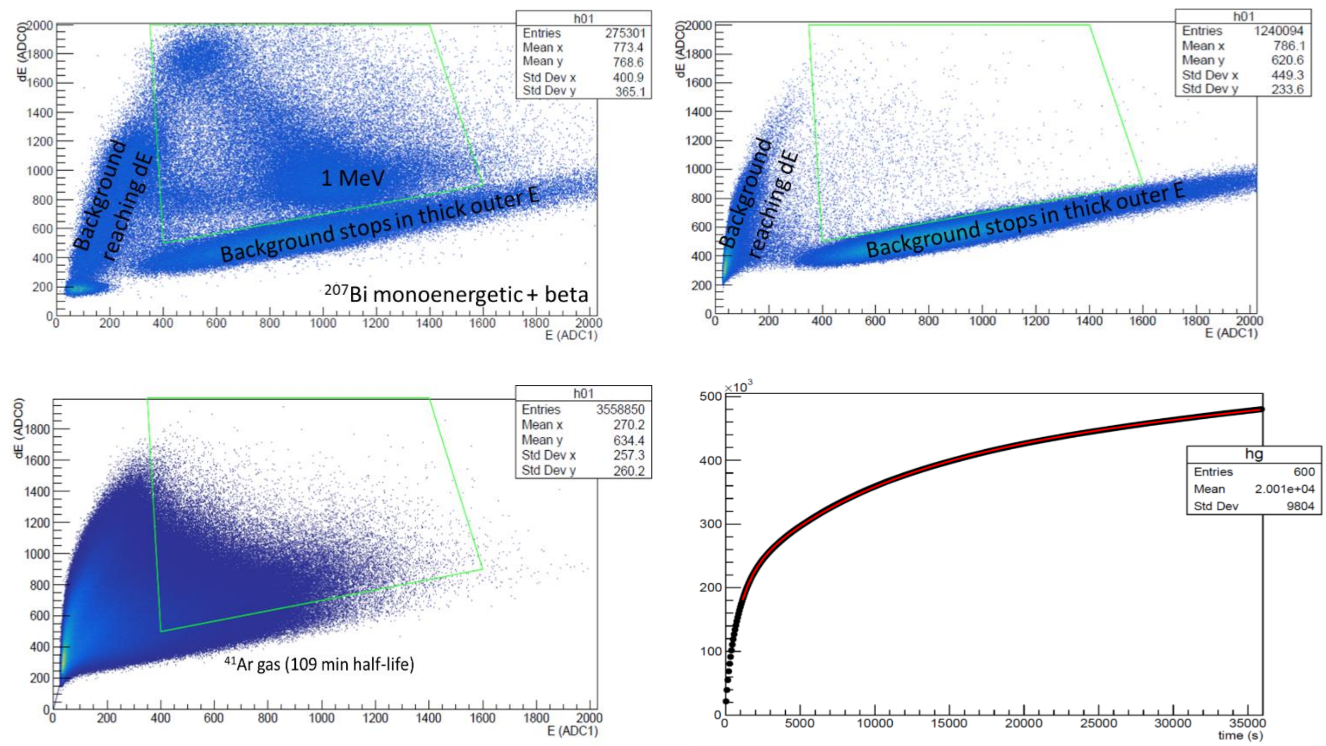

Figure 3. Results of the ^{40}Ar(d,p)^{41}Ar experiment. **(Top Left)** Inserting the ^{207}Bi source into the detector, which emits a beta spectrum and also approximately 1 MeV monoenergetic electrons, produced this 2D histogram, with the thin dE scintillator pulse height plotted on the vertical axis and the thick E scintillator pulse height on the horizontal axis. The 1 MeV electrons are clearly visible, as well as bands created by background radiation stopping in the thick E detector and reaching the dE. Events inside the green quadrilateral were considered to be electrons from the source. **(Top Right)** Same, but with the ^{207}Bi source removed. **(Bottom Left)** Same, but with the^{207}Bi source removed and the detector full of the ^{40}Ar/^{41}Ar gas mixture. Events inside the green quadrilateral were considered to be ^{41}Ar beta decays for the purpose of counting. **(Bottom Right)** Plotting the integral of the number of ^{41}Ar decays (events inside the green quadrilateral) (black circles) gives this growth curve, which was fit (red curve) by an exponential growth curve to obtain the decay constant and the initial number of ^{41}Ar, assuming all decays were detected.

IV. OMEGA Ride Along (December 2019)

A ride-along experiment was carried out during a series of high-yield DT shots on the OMEGA laser at the Laboratory for Laser Energetics on December 17, 2019 as a first attempt to address Q2 from Section II, that is, "What is the background rate?" As shown in Figure 4, in this experiment the getter-type detector and the turbopump trap detector were placed on the steel H-10 webbing of the OMEGA target chamber, approximately 2.4 m away from the target chamber center. The two detectors were placed side-by-side, and kept from moving by two lead bricks, one on each side. An aluminum plate bolted to the webbing kept the detectors from sliding backward. For some shots, lead bricks were placed in front of each detector. Each detector was connected to a Reynold 167-2669 high-voltage cable and an LMR-200 signal cable, which ran to the electronics located in the Cryocart 5 station in LeCave. The electronics only allowed a single detector to be tested at a time, so between shots the cables could be switched at the LeCave end to connect the desired detector. Switching also required the electronics to be re-tuned to the new detector, which required a ^{207}Bi source to be inserted.

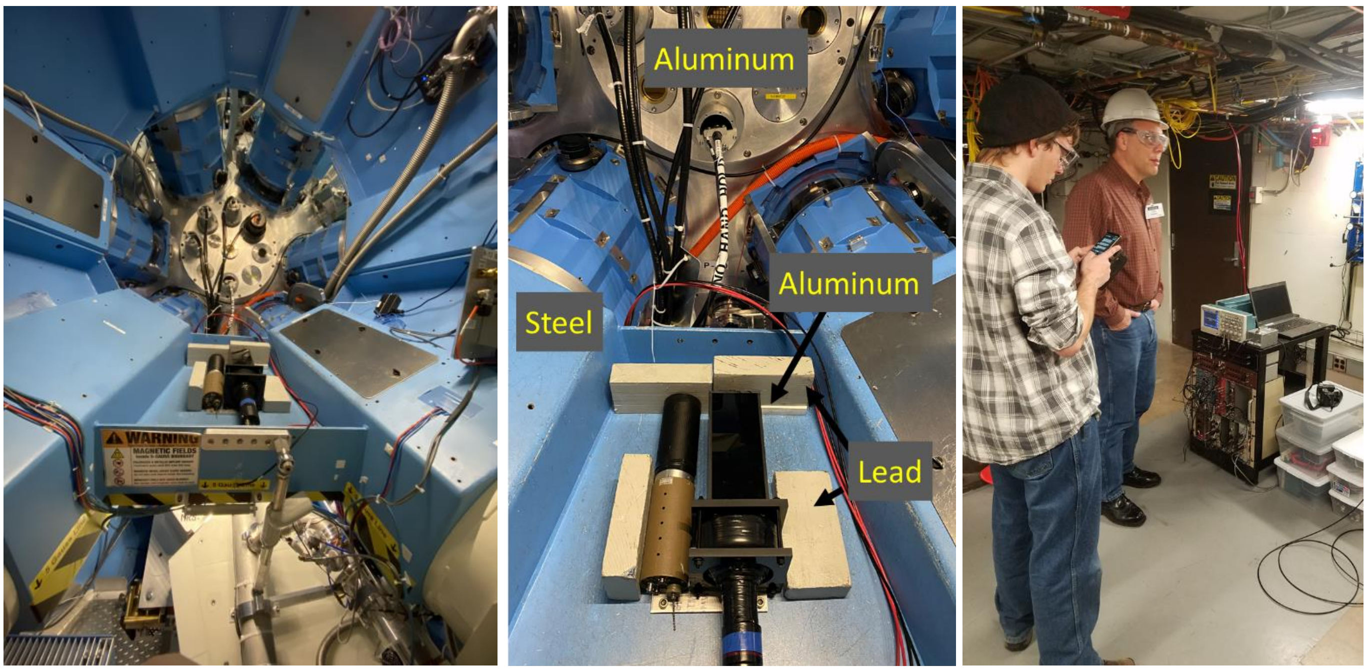

Figure 4. Set up for the OMEGA ride-along experiment. (Left) The two detectors were placed on the H-10 webbing approximately 2.4 m from the target chamber center. **(Center)** The smaller "getter trap" detector is on the left, the larger "turbopump trap" detector is on the right. A variety of materials that can be activated surrounded the detectors. **(Right)** Houghton College student Tyler Kowalewski and professor Mark Yuly prepared the electronics, located in LeCave near the Cryocart 5 location, used to process the signals from the detectors.

The top diagram in Figure 5 is a functional block diagram of the electronic controls for the experiment. A 400 ns TTL trigger signal from HTS LaCave(B) Crate was lengthened to about 5 μs in order to be used as the logic signal input to both an Arduino Mega 2560 Rev3 microcontroller and a FemtoDAQ acquisition system. When it detected the shot trigger, the Arduino was programmed to wait for 1 ms, then connect both the high voltage (HV) and HV ground to the detector using MOSFET switches to activate 15 kV high-voltage isolation reed relays. The circuit diagram for this is shown in Figure 14 in Ref. 11. At 2 ms after the shot another set of relays connected the signal and signal ground. The relays were used to prevent any voltage spike caused by the electromagnetic pulse (EMP) from damaging the HV power supply, PMT amplifier or linear fanout. The shot trigger also started the FemtoDAQ to begin data collection. In this way, $t = 0$ for data collection was only a few tens of nanoseconds after the shot, and the FemtoDAQ recorded pulse rates before, during and after the relays energizing and connecting the detectors.

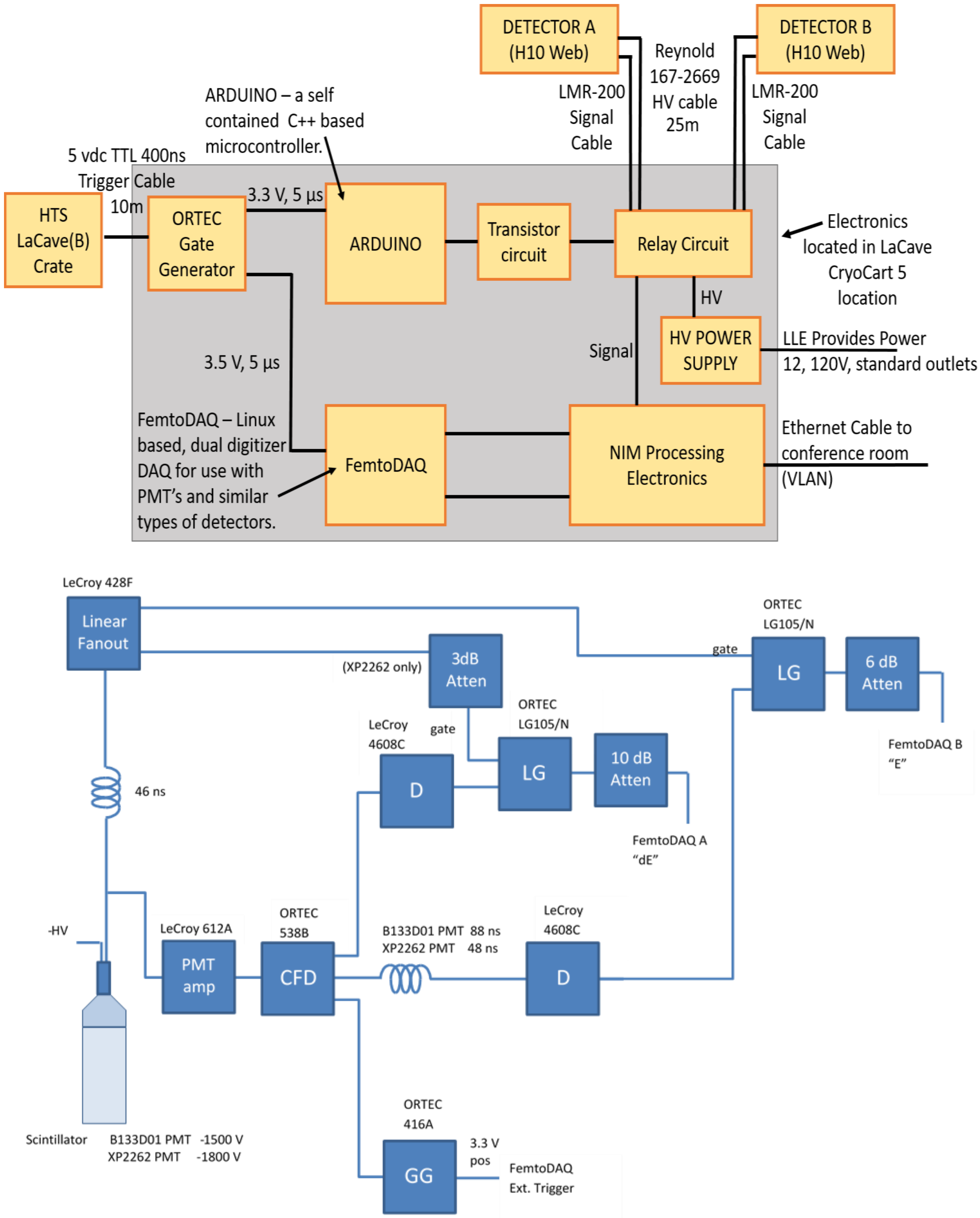

Figure 5. Electronics for the OMEGA ride-along experiment. (Top) Functional block diagram of the experiment controls and acquisition system. The shot signal triggered the Arduino to wait for 1 ms, close the relays that connect the high voltage and ground to the phototube, then wait another 1 ms before connecting the signal to the acquisition system. The same shot signal started the FemtoDAQ data acquisition, so time $\mathbf{t} = \mathbf{0}$ corresponded to a few tens of ns after the shot. **(Bottom)** The NIM electronics split the short dE pulse from the long E pulse for the turbopump detector (B133D01 phototube) and the getter detector (XP2262 phototube).

The bottom diagram in Figure 5 shows the NIM electronics used to process the pulses from the detector phototube. Since the detectors are phoswich detectors, the fast component of the pulse, created by the thin dE scintillator, needed to be separated electronically from the slow component from the thick E scintillator. The signal from the PMT was initially split to two parts, one part to become the analog input for the linear gates, and the other to form the logic gate used by the linear gate to select the fast or slow component of the analog pulse. The latter signal was amplified (LeCroy 612A) by a factor of 10 so that the constant fraction discriminator (CFD) could trigger on the smallest pulses, those just slightly larger than the phototube noise. The width of logic gate from the CFD for selecting the fast component of the PMT pulse was about 70 ns for both detectors. The 50 ns wide logic gate for the slow component was delayed by 88 ns for the turbopump trap detector and 48 ns for the getter detector. The linear gates (EG&G LG105/N) integrate the pulses and hold the value for approximately 3.5 µs. The analog signals input to the linear gate and the linear gate outputs themselves were attenuated in order to make them compatible with the -1 V to 1 V inputs on the FemtoDAQ.

One significant drawback to using the LG105/N linear gates, which date back to the 1960's, is the long hold time. This causes an unusual form of pileup to occur. If additional pulses come within 3.5 µs of the first, the event will be recorded with the correct timestamp but the recorded pulse height information will be the same as the previous event. In order to correct for this for the getter detector, for any events coming within 3.5 µs of each other only the first was kept, the remainder were discarded. At high count rates this noticeably increased the dead time but improved the ability to use the 2D histograms for particle identification. Particle identification and deadtime corrections were not attempted on the turbopump trap detector because of the poor quality of the spectra due to the high rates.

The FemtoDAQ uses an FPGA to sample and digitize the voltage at each input every 10 ns. Once started by the leading edge of the external gate input, the FPGA in the FemtoDAQ continued to sample both channels every 10 ns for 350 ns, computed a running average over four samples, then recorded the maximum value of the running average in memory, along with a timestamp. Because of the limited memory available on the FPGA, only 65,535 events can be recorded in memory before they have to be read out into the Linux-based BeagleBone Black computer inside the FemtoDAQ. Moreover, since the 32-bit time stamp records the number of 10 ns "clocks" since $t = 0$, the maximum duration before reading out the FPGA is 42.9 s. Although the FPGA incurs very little deadtime while it is collecting, the process of transferring data to the BeagleBone is extremely slow. It would be advantageous to either find a way to keep the total number of recorded events during the first few half-lives below 65k using shielding or some other method, or find another device like the FemtoDAQ but with more FPGA memory.

As shown in Table 2, an attempt was made to collect data from eight laser shots; four of them were successful. On the very first shot of the day the FemtoDAQ crashed right when the shot occurred, perhaps because of a power surge. On the second attempt, everything worked perfectly except the relays to power up the phototube did not close. In other failed attempts the FemtoDAQ started data collection then hung, perhaps when the memory was filled, and once the FemtoDAQ did not begin data collection even though the shot happened and the Arduino turned on the detector.

In the first successful attempt, shot 96181 shown in Figure 6, the FemtoDAQ timeout was set to 30 s. Because the count rate was so high (over 350k/s), however, the FPGA buffer filled quickly, forcing the FPGA to read out into the BeagleBone computer after only 0.5 s rather than 30 s. Apparently, overflowing the memory causes the time required to read out the FPGA memory to be even longer than normal, and in this case it took 4 s! For the second successful attempt, shot 96184, also shown in Figure 6, the timeout for the FemtoDAQ was reduced to 0.2 s, short enough so that the FPGA did not have unexpected timeouts due to overflowing the memory. This reduced the required readout time to about 1.2 s, which is still long but less than would be expected from the difference in the total number of stored events.

Table 2. List of Laser Shots. There were four shots in which useable data were obtained (highlighted orange), three using the turbopump trap detector and one with the getter detector.

Shot Number	Neutron Yield	T_{ion} (keV)	Detector	Shielding	FemtoDAQ Timeout	Note
96175	1.04×10^{14}	9.28	turbotrap	none		FemtoDAQ crashed
96178			turbotrap	none		Trigger test, null shot
96179	1.34×10^{14}	9.51	turbotrap	none		Relays failed to close, FemtoDAQ okay
96080			turbotrap	none		Trigger test, null shot
96181	1.32×10^{14}	8.44	turbotrap	none	30 sec	Good
96183			turbotrap	none	30 sec	No data, FemtoDAQ memory filled?
96184	1.56×10^{14}	10.64	turbotrap	none	0.2 sec	Good
96185	1.50×10^{14}	8.68	turbotrap	lead	0.2 sec	Good
96186			getter	lead		No FemtoDAQ trigger
96187			getter	lead		Trigger test, null shot
96188			getter	lead	30 sec	Good

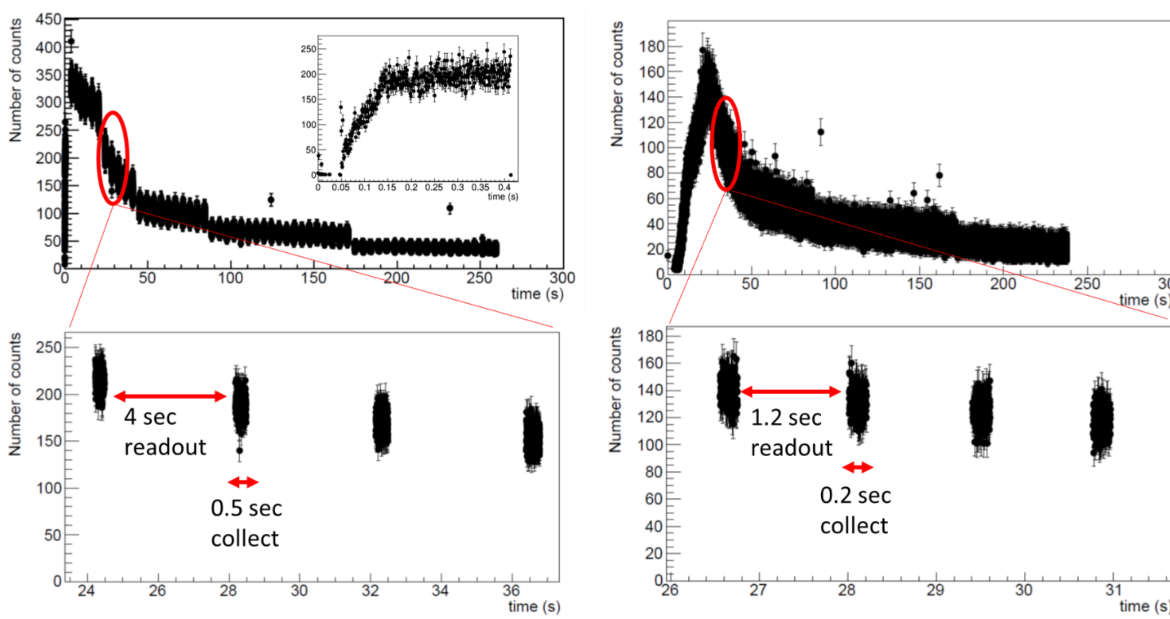

Figure 6. Raw decay curves obtained from the large turbopump trap detector. (Left side) The decay curve (top) for shot 96181, with 1 ms time bins and not corrected for deadtime, shows the data acquisition system struggling to handle the extremely high count rates of greater than 350,000 events/s. The inset shows the detector reached maximum event rate as early as 200 ms after the shot. As can be seen in the plot showing just the period from 24 to 36 s (bottom), at this rate the buffer filled after only about 0.5 s, and took about 4 s to read out before data collection could resume. **(Right side)** For shot 96184 (top) the FemtoDAQ timeout was set to 0.2 s, which allowed the data acquisition system to keep up better but inexplicably delayed the maximum event rate to about 25 s after the shot. As seen for the period from about 26 to 31 s (bottom) the buffer did not fill prior to the 0.2 s timeout, and the readout time was 1.2 s.

There was only one successful shot using the getter detector, shot 96188, which had a much lower maximum count rate, about 18,000 events/s, due to its much smaller volume. Because of this, the FemtoDAQ had no problem keeping up and it was possible to correct for deadtime, as shown in Figure 7. The FemtoDAQ timeout was 30 s, which was long enough that the buffer filled prematurely only once, at about 7 s, thereafter reading out every 30 s. When turning on, the detector did not reach maximum count rate until about 0.2 s.

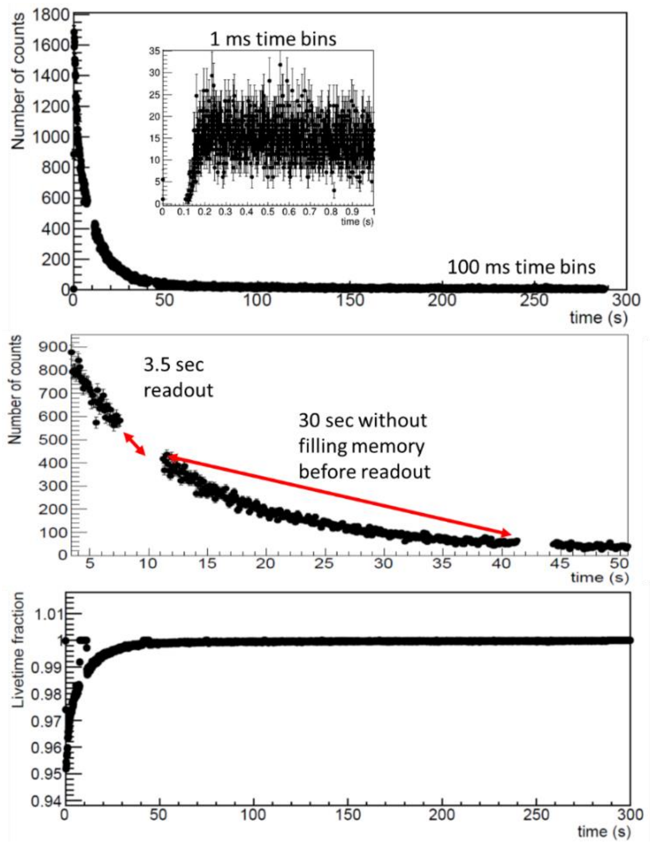

Figure 7. Decay curves obtained from the small getter detector. (Top) The getter collector decay curve, with 100 ms time bins, for shot 96188, with a lead brick in front of the detector and the FemtoDAQ timeout set to 30 s. **(Inset)** The first second of the decay curve with 1 ms time bins. The count rate reaches a maximum of about 18,000 events/s at about 0.2 s. **(Middle)** Plot of the time interval from 5 s to 50 s. The FPGA buffer does not fill and the FemtoDAQ takes 3.5 s to read out after the set timeout of 30 s. **(Bottom)** Event-by event livetime calculation as a function of time. Even at the highest count rate the livetime was still about 95%. The readout interval, which, of course, contributes to the overall livetime, is ignored.

Figure 8 compares the 2D energy histograms for the large turbopump trap detector and the small getter detector. The much lower rates in the getter detector allow the background to be easily separated. Prior to the shot, in each case a calibration histogram was made using a ^{207}Bi source. This allowed good beta decay events to be identified as those falling within the red quadrilateral. Finally, the count rate as a function of time, corrected for deadtime and "pileup", for both all events and good beta decay events could be plotted and fit with a sum of decaying exponentials plus a flat background (Figure 9). The resulting fit parameters are shown in Table 3. It was found that when all events are included a good fit to the resulting decay curve could only be obtained with three decaying exponential components were included, with half-lives around 0.7 s, 7 s and 60 s. When only the good beta events were included in the fit, the 60 s component was not needed.

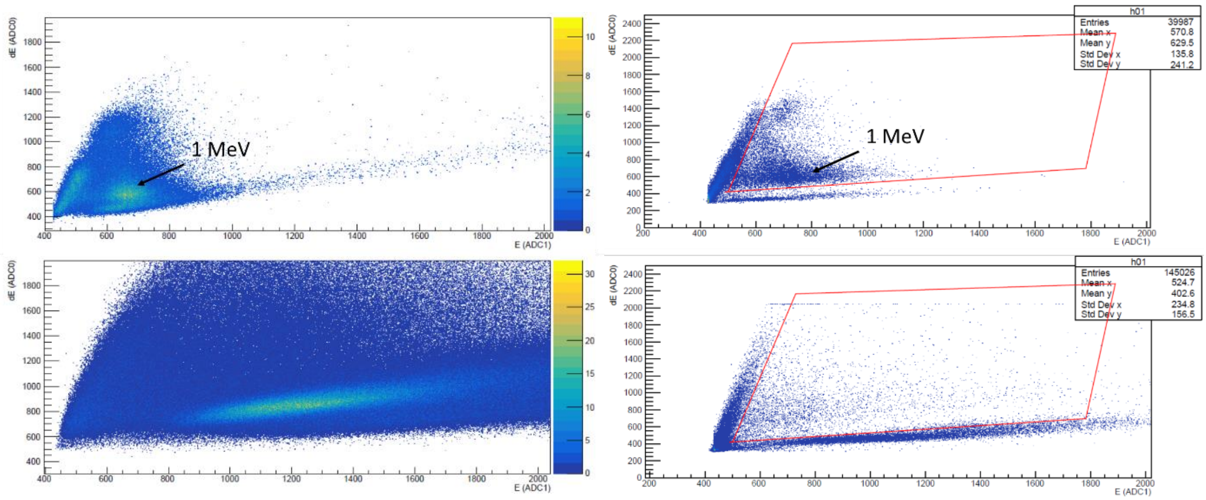

Figure 8. 2D Histograms for Turbopump trap and Getter detectors. (Left side) The 2D histograms for the turbopump detector with dE pulse height on the vertical and E pulse height on the horizontal axis, for the ^{207}Bi source (top) and shot 96184 (bottom). **(Right side)** Same, but for the smaller getter trap detector and shot 96188. The red quadrilateral is the cut on beta particles.

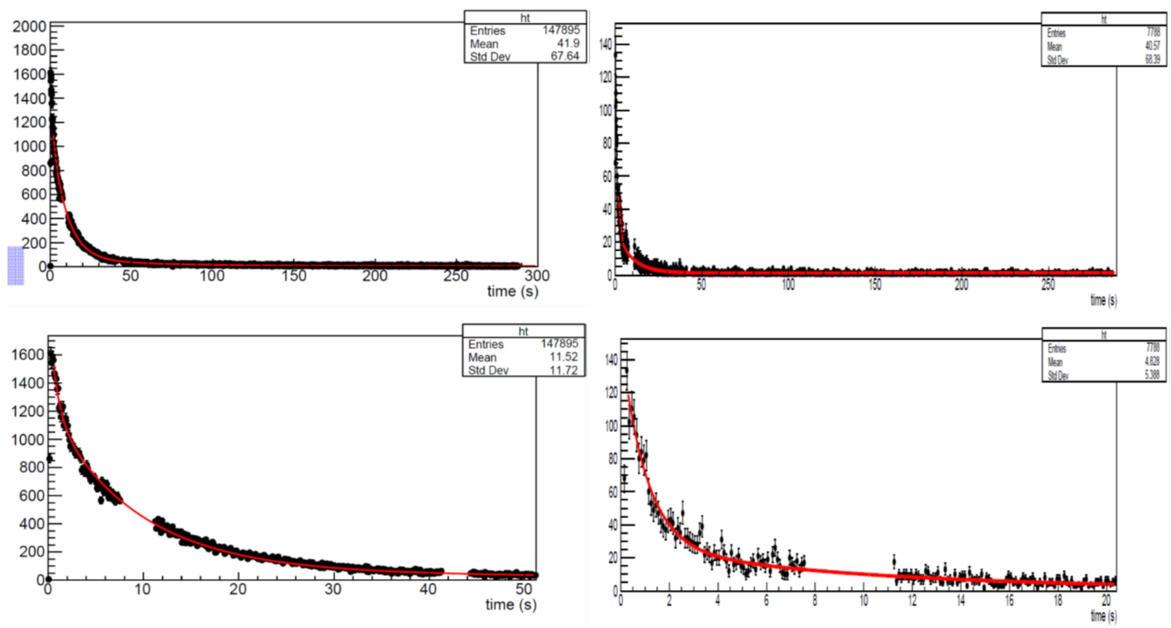

Figure 9. Decay curve fits. (Left side) Fit of exponential decay functions plus a flat background to the raw getter detector rate as a function of time for shot 96188, showing full 300 s interval (top) and the first 50 s (bottom). Three exponential functions were needed before a good fit could be obtained, with approximate half-lives of 0.7 s, 7 s, and 60 s. **(Right side)** Same, except for the fit is to the beta decay rate corresponding to good beta events inside the red quadrilateral in Figure 8. In this case, the long 60 s half-life component was not needed to obtain a good fit.

The most likely source of this radiation, which will be background in an actual experiment trying to measure the number of product nuclei produced in nuclear reactions occurring in an ICF implosion, is being investigated. Two candidates have been found for the 7 s component, ^{27}Al(n,2n)^{26}Al* with a half-life of 6.35 s and ^{16}O(n,p)^{16}N with a half-life of 7.13 s. The cross sections for both of these reactions is relatively high and both materials were present nearby. The detectors were wrapped with a thin aluminum foil in order to keep light from escaping the detector, one of the lead bricks was on an aluminum plate, and the OMEGA target chamber itself is a 1.6 m radius aluminum sphere, the wall of which was only

81 cm from the detectors. The first excited state of ^{26}Al is a 0+ state with a half-life of 6.34 s. If the $^{27}Al(n,2n)^{26}Al^*$ reaction leaves the ^{26}Al this metastable state it will beta decay to the ground state of ^{26}Mg [16]. The $^{16}O(n,p)^{16}N$ reaction would occur in air around the detector and inside the turbopump trap detector, with the ^{16}N beta decay occurring about 66% of the time to the 6130 keV state, 10% to the 6049 keV state, 9% to the ground state and the rest to other excited states of ^{16}O [17]. The excited states of ^{16}O would then decay by gamma ray emission. The source of the 0.6 s and 40 s components is currently unknown.

Table 3. Best fit parameters for the getter detector. Fit parameters for the getter detector decay curve as a function of time for shot 96188 both for raw count rate and for beta particles, selected using the red quadrilateral in Figure 8.

Raw count rate		**Beta particles**	
$T_{1/2}$ (sec)	N	$T_{1/2}$ (sec)	N
0.76	728	0.73	115
7.13 (fixed)	1080	7.13 (fixed)	23
59	40	Not needed	

In Table 1 it was found that the light ion reactions of interest would yield between approximately 10^5 to 10^7 product nuclei per shot. Assuming that the fraction trapped would be about 1%, which is consistent with the solid angle of the detector assuming the detector is otherwise 100% efficient, then for a one-second half-life product nucleus the number of decays in the trap in the first half-life would be 500 to 50,000. The answer to Q2 “Is the low background rate after the shot low enough?” would appear to be, to first order, yes for the getter detector and no for the turbopump trap detector. However, in an actual experiment the getter detector would be located inside the target chamber not outside, no air would be present inside the turbopump trap detector, and the turbopump trap detector would undoubtedly be shielded. Moreover, much improvement can still be made to the speed of the electronic readout of the detectors which would reduce pileup and improve particle identification.

V. Geant4 Simulations

A Geant4 [18] code to simulate both the turbopump trap detector and the getter detector has been written in collaboration with Ryan Fitzgerald from the NIST to model the response of the detectors to a variety of different radiation sources. This simulation will allow the absolute efficiency of both detectors to be calculated (Q1 (b)) as well as allow the relative contribution of different background sources to be explored. Shielding configurations could also be optimized this way.

As it is currently configured (for example, see Figure 10 top left), only the thin, fast dE scintillator and the thin, slow E scintillator are included in the model for each detector, plus the steel vacuum port in the case of the turbopump trap detector. Air surrounds the detector, and is inside the detector for the turbopump trap detector. An aluminum plate is positioned near the front of the turbopump trap detector. One item that is currently not simulated, but which is undoubtedly a significant source of background is the aluminum foil that wraps each detector. In the future, it may also be possible for the code to simulate the actual pulse of primary DT neutrons from the implosion, and follow these neutrons as they activate the materials surrounding the detector. This would have the advantage of possibly allowing unexpected background sources to be identified.

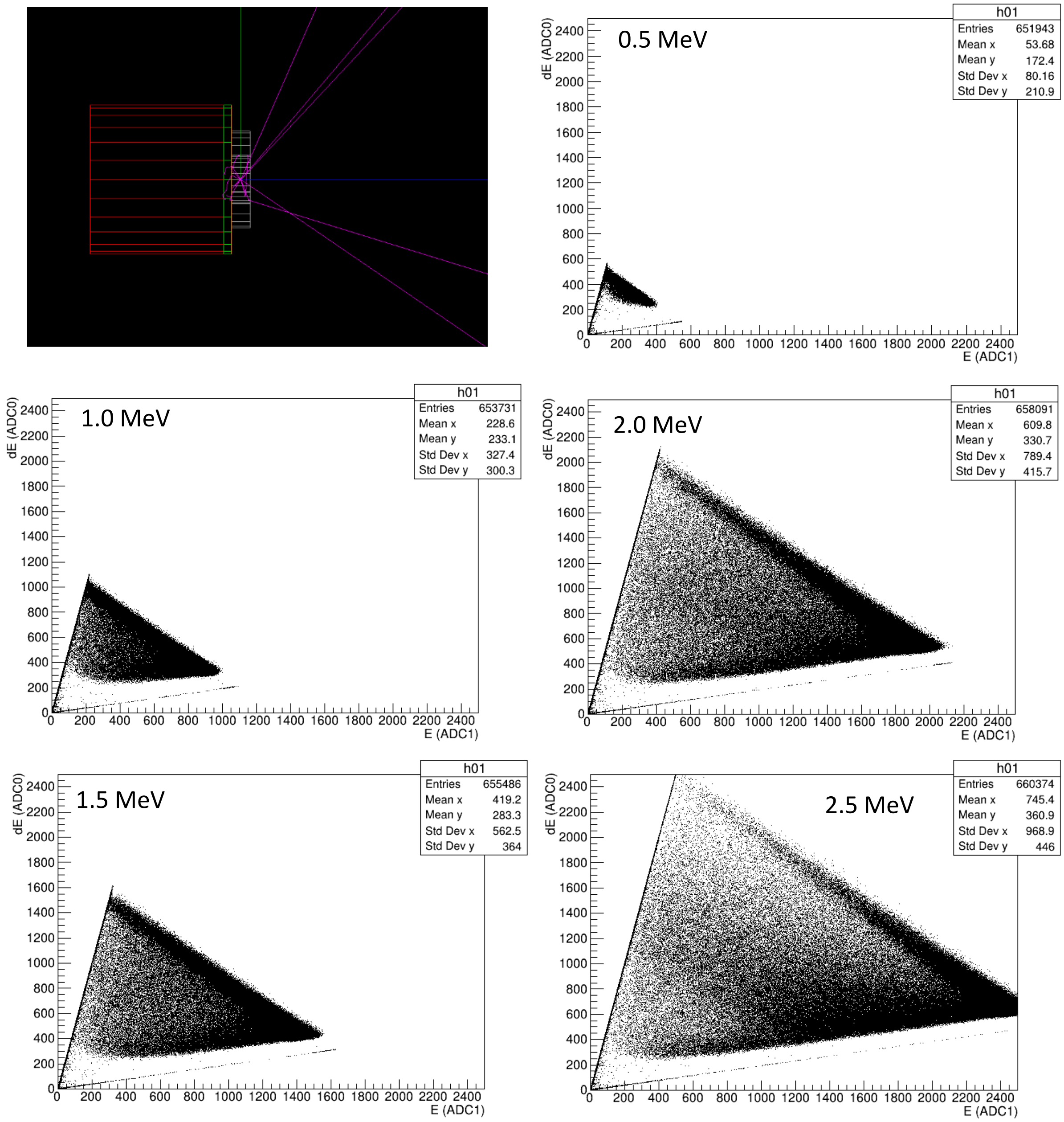

Figure 10. (Top Left) Geometry for the Geant4 simulation of the small "getter" detector. In this case, a monoenergetic electron point source is located directly against the thin dE detector so that electrons can enter the detector over a wide range of angles. Because of this, a range of energies can be deposited in the dE detector, from the least when the electron travels perpendicular to the detector to all of the electron's energy when its path is almost parallel. **(Remaining Panels)** The resulting 2D energy histograms for monoenergetic electrons of 0.5, 1.0, 1.5, 2.0 and 2.5 MeV.

Several possible radiation sources can be selected. The ^{207}Bi source that is used to calibrate the detectors has been simulated, including the mylar film inside of which the ^{207}Bi is deposited and the steel ring holding the mylar. This detector can be moved around and the resulting detector response can be simulated. It is also possible to simulate the decay of any other radioisotopes in the various volumes defined in the code. For example, decays of ^{16}N distributed randomly in the air outside or inside the detector can be simulated, or ^{26}Al* decays in the aluminum plate. Finally, artificial particle sources, such as an isotropic point source of monoenergetic electrons, for example, can be simulated.

After the simulated decay of the source nucleus or the generation of the artificial particle event, the code tracks the particle and the various daughters as they interact with materials in the vicinity, until they either stop or interact with the detector. It then records the total energy deposited by all particles into each scintillator. For a radioisotope source, it can also record the time after the shot the decay occurred. The simulation code generates a list file that is nearly identical to the list file generated by the python code running the FemtoDAQ that collects the data in an actual measurement. The file is simply an event-by-event list containing the timestamp and pulse heights from the dE and E detectors. Since the format is the same, the output from the Geant4 simulation can be read into and analyzed using the same ROOT [19] analysis code used to analyze the data from the experiment.

As an example, Figure 10 shows simulation 2D histograms for a monoenergetic electron point source located right at the center of the front face of the dE scintillator on the getter trap, as drawn in the upper left. For each electron energy, the electrons fall into a triangular band that increases in size with energy. The rightmost corner corresponds to electrons striking perpendicular to the dE scintillator, losing a minimal amount of energy in the dE and depositing most of their energy in the E scintillator. This was confirmed by simulating a collimated beam of electrons string perpendicular to the dE detector. The band moving from this corner upward to the left results from electrons striking the surface at greater and greater angles and depositing more and more energy in the dE until finally they do not reach the E scintillator at all. This is the top corner of the triangular band. The band moving downward and to the left from the rightmost corner is most likely due to electrons scattering from other things before entering the detector.

Figure 11 shows a comparison of the simulated detector response to the actual detector spectra for a ^{207}Bi source located inside the large turbopump trap detector. It is clear that the simulation captures many of the features, but is not identical to the measurement. This is most likely because the simulation only tallies the total energy deposited in

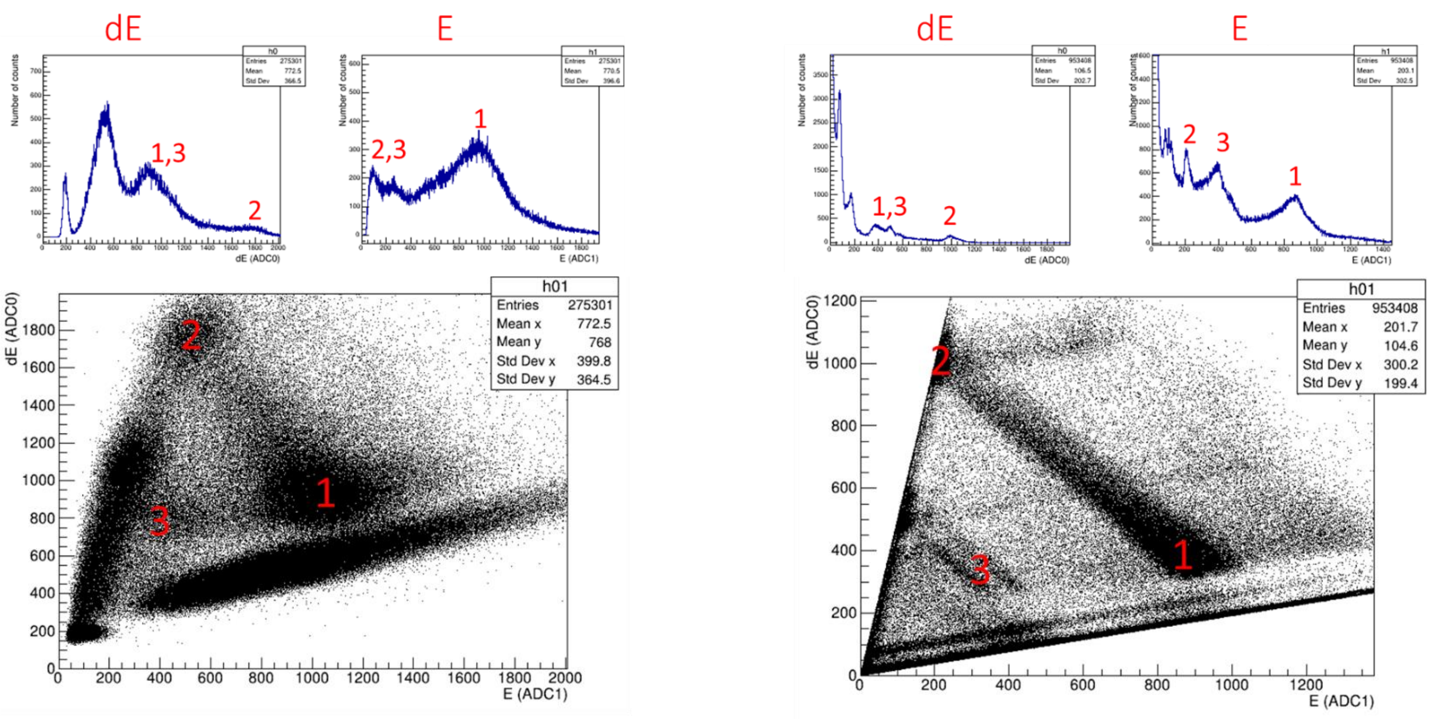

Figure 11. Comparison of Geant4 simulation with data. (Left) Singles energy spectra for the dE and E scintillators (top) and the corresponding 2D histogram (bottom) with a ^{207}Bi source inside of the turbopump trap detector. **(Right)** Geant4 simulation of the same situation. Corresponding features are numbered, (1) 976 MeV ^{207}Bi electrons, (2) 976 MeV electrons entering the dE detector very obliquely, 482 keV ^{207}Bi electrons.

each scintillator but does not simulate actual detector response – for example, attenuation of the visible light traveling in the scintillator and light guide, PMT noise, electronic separation of the fast/slow components, etc. Shared features in the 2D histograms numbered. Feature (1) corresponds to the approximately 1 MeV monoenergetic electrons emitted by ^{207}Bi. Feature (2) is 1 MeV electrons that deposit most or all of their energy in the dE detector because of their angle of incidence. Feature (3) is the ^{207}Bi electron peaks at approximately 0.5 MeV. Careful study of these histograms reveals that the lower part of the dE and E detector energy spectra are cut off because of the threshold required for triggering – cutting off the low energy detail present in the simulation. It also appears that the measured spectra may be shifted due to the offset and bias settings of the linear gates.

Table 4 shows very preliminary results for the predictions of the Geant4 simulation for the background in each detector due to the $^{16}O(n,p)^{16}N$ reaction occurring in air. In each case, the expected number ^{16}N nuclei created in the $^{16}O(n,p)^{16}N$ reactions that would occur in the given volume was calculated by hand from the known cross section and the neutron yield for the laser shot. The designated volume of air was either the 400 mm cube simulation volume for Geant4, or the volume inside the turbopump trap detector. The Geant4 simulation was used to determine the number of events that would be detected for one million ^{16}N nuclei distributed randomly throughout the volume. This result was then scaled by the calculated number of ^{16}N produced in the laser shot to give the predicted total number of ^{16}N detected decays per shot. Assuming the 16N decays exponentially with a 7.13 s half-life, it is then possible to calculate the expected number of decays in a 1 ms interval at a given time after the shot. For the getter trap detector, since the ride-along measurement was clean enough, a “good beta event” cut was made on both the measured data and the Geant4 simulated data.

Interestingly, Table 4 indicates that for both detectors, and for air both inside and outside the turbopump detector, the expected number of background counts due to $^{16}O(n,p)^{16}N$ is roughly the same. For the getter detector data, in which actual beta events were selected, the measured number of detected events is slightly lower than the prediction, which is impossible since we know other background sources besides $^{16}O(n,p)^{16}N$ must also be present. In particular, the detector is wrapped in aluminum foil so $^{27}Al(n,2n)^{26}Al^*$ should generate beta radiation. Nevertheless, the close agreement may mean that these other sources are small. For the turbopump trap detector, the measured total rates (i.e. not cut on good electrons) both from air both inside and outside the detector was approximately the same in both cases, about four times the predicted rate, which would make sense if background from other sources was also present.

Table 4. Preliminary Geant4 simulation results for $^{16}O(n,p)^{16}N$ background.

	Getter Trap From air outside Shot 96188 Cut on beta events		Turbopump trap From air inside Shot 96184	Turbopump trap From air outside Shot 96184
Calculated ^{16}N per shot	1.6×10^9		1.1×10^7	1.6×10^9
Geant4 predicted ^{16}N detected decays per million ^{16}N	155		476,655	4,500
Predicted total ^{16}N detected decays per shot	245,365		5,419,567	7,024,500
	(at t= 0.2 s)		(at t= 30 s)	
Detected decays expected in 1 ms	23		29	37
Detected decays measured in 1 ms	~18		~120	~120

The 400 mm cube Geant4 simulation volume may be too small to obtain an accurate prediction for the contribution from air outside the detector. This needs to be further studied.

VI. Planned Exploding Wire Experiments

Presently the only way to address Q1 (a), "How do we know what fraction of the product nuclei were collected?" is by experiment. To this end, we are collaborating with James McLean and his students Vizma Leimanis and Pranish Shrestha from SUNY Geneseo to design a device to quickly release a radioactive gas isotropically in our test vacuum chamber, which has been reconfigured for this experiment.

The experiment will be carried out using the 30R beamline on the 1.7 MV tandem Pelletron at SUNY Geneseo. As shown in Figure 12, the test chamber will be taken from Houghton College to SUNY Geneseo and placed downstream of the current 30R scattering chamber. Deuterons from the accelerator will cross the current scattering chamber and enter the test chamber where they will strike a wire or foil target. The wire or foil will be composed of or coated with a substance that will become activated by deuterons or possibly neutrons. Several ideas are under consideration.

1. A solid wire composed of the correct material could be activated directly by the deuteron beam, then caused to explode by a short high-current pulse. Problems with this technique include possibly only vaporizing a small portion of the wire, incomplete vaporization leading to small bits of solid or liquid being sprayed into the chamber to possibly foul the turbopump, and the requirement that the material be a conductor.'
2. A solid wire could be coated with the desired substance and caused to explode by a large current pulse. This would allow non-conducting materials to be used, but the other problems remain.
3. A solid wire could be coated with the material, then the wire could be quickly heated, causing the coating to rapidly evaporate. This would eliminate the possibility incomplete vaporization, if it could be done quickly enough.
4. For pure substances having undesirable properties (i.e. vapor pressure too low) chemical compounds containing the desired nucleus could be used.
5. Initially, a flat foil could be used in place of the wire, since it would be easier to achieve maximum activation with the finite-sized beam spot. However, for isotropy measurements the wire would be needed, and it may be necessary to rotate the wire to achieve greater cylindrical symmetry of the activated material.
6. For neutron reactions, the wire could be coated with deuterated polyethylene to produce neutrons when struck by the deuteron beam.
7. Wires could be coated using vacuum deposition, electroplating, or simply dipping in molten material, whichever is most suitable for the particular substance.

Candidate materials and reactions are listed in Table 5. These have been selected for giving the largest yields with the most useful electrical and thermal properties. Only candidates with half-lives between about 1 s and 1 h were considered. Although the $^{19}\mathrm{F}(\mathrm{n},\alpha)^{16}\mathrm{N}$ reaction has a significantly lower yield, it was selected as being the best reaction yielding a short-lived product, ^{16}N, with a 7.13 s half-life.

In order to carry out the exploding wire experiments, several modifications were made to the test chamber, the traps and detectors this past summer.

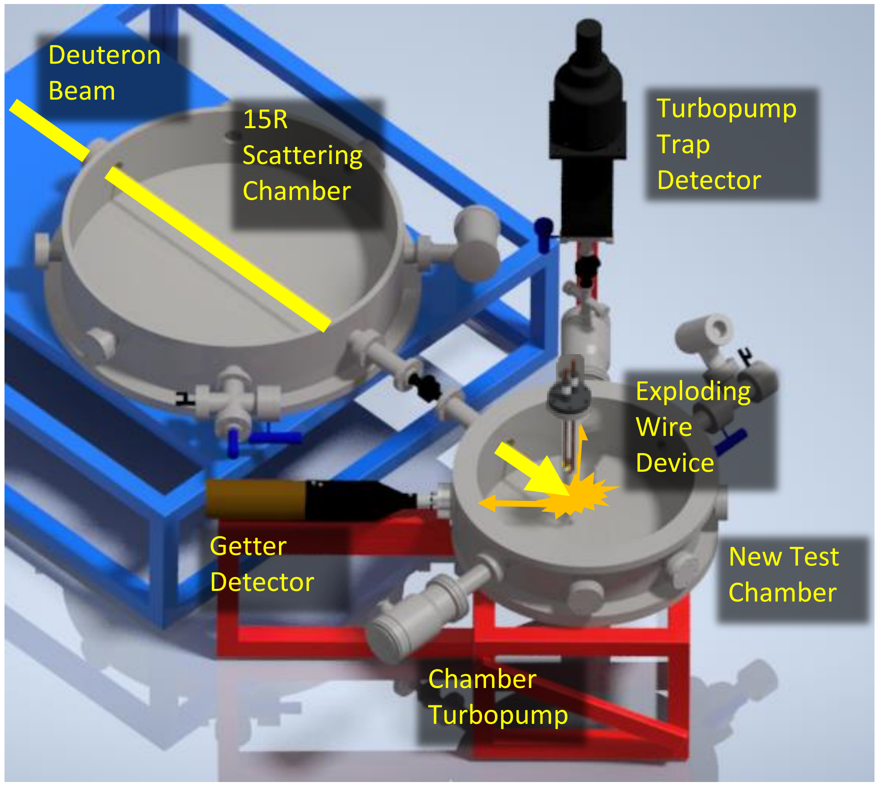

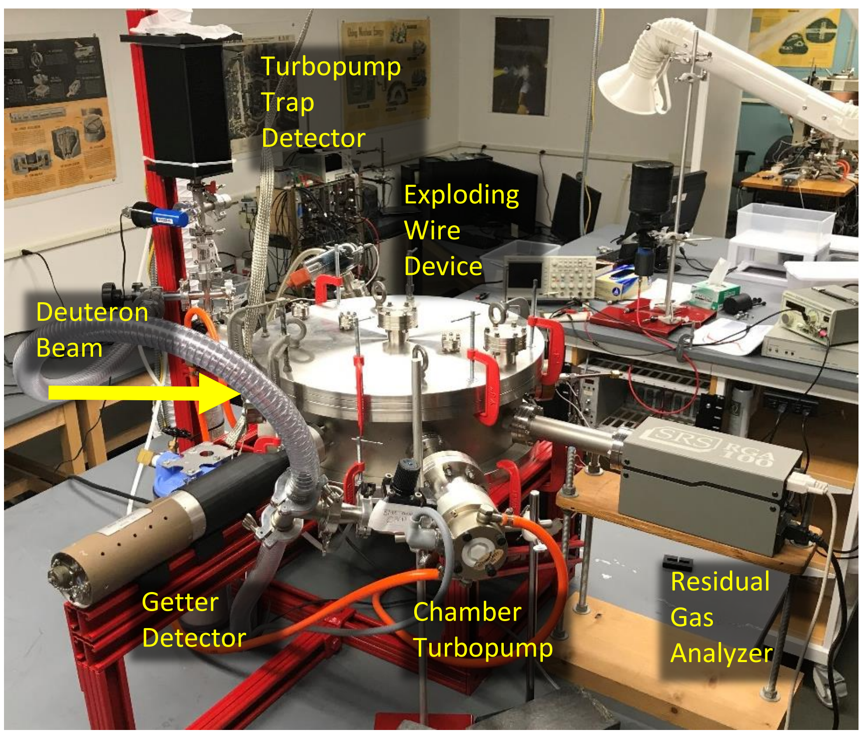

Figure 12. Exploding Wire Experiment. (Top) 3D CAD drawing of the SUNY Geneseo Pelletron 30R beamline, showing the new test chamber attached to the downstream side of the 30R scattering chamber. The deuteron beam will cross the 30R scattering chamber, enter the test chamber, and strike a wire or foil target. The wire or foil, or a coating on the wire or foil, will become activated. After a period of time, the beam will be cut and a large current passed through the foil or wire, causing it to explode or quickly evaporate the radioactive material. This vaporized material will then be collected, trapped and counted by the getter detector and turbopump detector. **(Bottom)** Photograph of the test chamber under assembly at Houghton.

Table 5. Candidates reactions under consideration for the exploding wire experiment. Assumed properties of the deuteron beam used in the yield estimates are shown in orange. The maximum yield shown occurs when the rate of product decay is equal to the rate of production.

Reaction	Reaction Threshold (MeV)	Reactant Natural Abundance (%)	Approx. Cross-Section (barns)	Product Half-Life (s)	Product Beta End Point Energy (MeV)	Yield (Total Number of Product Nuclei)
Deuteron Reaction: Deuteron beam 10 nA, Deuterons/second = 6.25 x 10^{10}, 2 MeV						
$^{27}Al(d,p)^{28}Al$	0.0	100	1.5 x 10^{-1}	134.7	2.8	3.3 x 10^{7}
$^{65}Cu(d,p)^{66}Cu$	0.0	31	6.5 x 10^{-2}	307.2	2.6	5.2 x 10^{6}
Neutron Reaction: Deuteron beam 10 nA, Deuterons/second = 6.25 x 10^{10}, 2 MeV; Neutron Energy = 5 MeV, neutrons/second = 3.87 x 10^{6}						
$^{19}F(n,\alpha)^{16}N$	1.6	100	2.1 x 10^{-1}	7.1	4.2	1.6 x 10^{4}
$^{55}Mn(n,p)^{55}Cr$	1.9	100	2.0 x 10^{-2}	209.8	2.6	2.6 x 10^{5}
$^{27}Al(n,p)^{27}Mg$	1.9	100	2.0 x 10^{-3}	567.4	1.7	1.3 x 10^{4}

1. **Turbopump trap.** A structure for mounting the turbopump trap detector (see Figure 13 b, c, d) was built using unistrut. The turbopump itself was rotated so that the outlet port faced upward, and the detector was attached. Provision was made for attaching a thermocouple gauge and a pneumatic valve between the turbopump and the detector so that the detector can be quickly isolated, trapping the gas within, and so that the pressure in the detector can be monitored. In addition, the 5-inch ADIT B133D01 phototube was replaced with an ET Enterprises 9823KB phototube having better gain and speed. To do this, a new PMT base was constructed. Interestingly, it seems like the speed of the 9823KB is such that for the slow scintillator, when the light intensity is low and spread out over hundreds of nanoseconds, pulses from individual photons are resolved whereas with the B133D01, which was not designed with speed in mind, the bandwidth is low enough that the slow pulses run together. Individual pulses for each photon will not work well with the current electronics, which is expecting a fast pulse followed by a long tail. Traditionally, in cases like this, a low-pass filter (or integrator) is used to create a single pulse with area proportional to the sum of the individual photon pulses. This is being attempted, but has the problem that any low-pass filter that can integrate the individual photon pulses also seems to obliterate the pulse from the fast scintillator. To use the 9823KB tube, we may need to completely redesign the electronics, or we may decide to go back to the old B133D01 tube.

2. **Getter trap.** In order to use the getter detector, a 362 mm (14.25 inch) long, 9.5 mm (3/8 inch) diameter acrylic rod was inserted between the phoswich detector and the photomultiplier tube (see Figure 13 a, b). The ends of this light guide were polished by first using progressively finer grades of sandpaper, then using Novus 7100 plastic polish. The phoswich detector itself consisted of a 15 mm long, 10 mm diameter cylinder of slow EJ-240 scintillator, and a 1 mm thick, 9.5 mm (3/8 inch) diameter fast EJ-212 scintillator. The scintillators were optically and physically coupled to each other and the light guide using Eljen Technologies EJ-500 optical epoxy. In order for the lightguide to penetrate into the vacuum, a special 2.75-inch conflat feedthrough was made out of aluminum. The lightguide passed through a hole in the feedthrough, and was sealed by a #110 Viton O-ring that was compressed by a smaller,

33.85 mm (1.33 inch) flange. The lightguide was optically coupled to the XP 2262 phototube using Eljen Technologies EJ-550 optical grade silicone grease, and held in place using a plastic 3D-printed holder that also serves as a light tight seal. To support the detector and PMT such that the detector could be located inside the vacuum chamber, a unistrut mounting frame was built.

Tests using the getter detector seemed to show a significant reduction in the amount of light reaching the PMT from when the scintillator was directly coupled to the PMT without the lightguide. Future work is needed to determine the reason for the reduction in light – whether it is due to the lightguide absorbing the light, light escaping from the detector or lightguide, the optical couplings, or some other reason. If the lightguide is absorbing the light it may be possible to replace the acrylic rod with a higher quality rod, a commercial light pipe, or even a bundle of fiber optics.

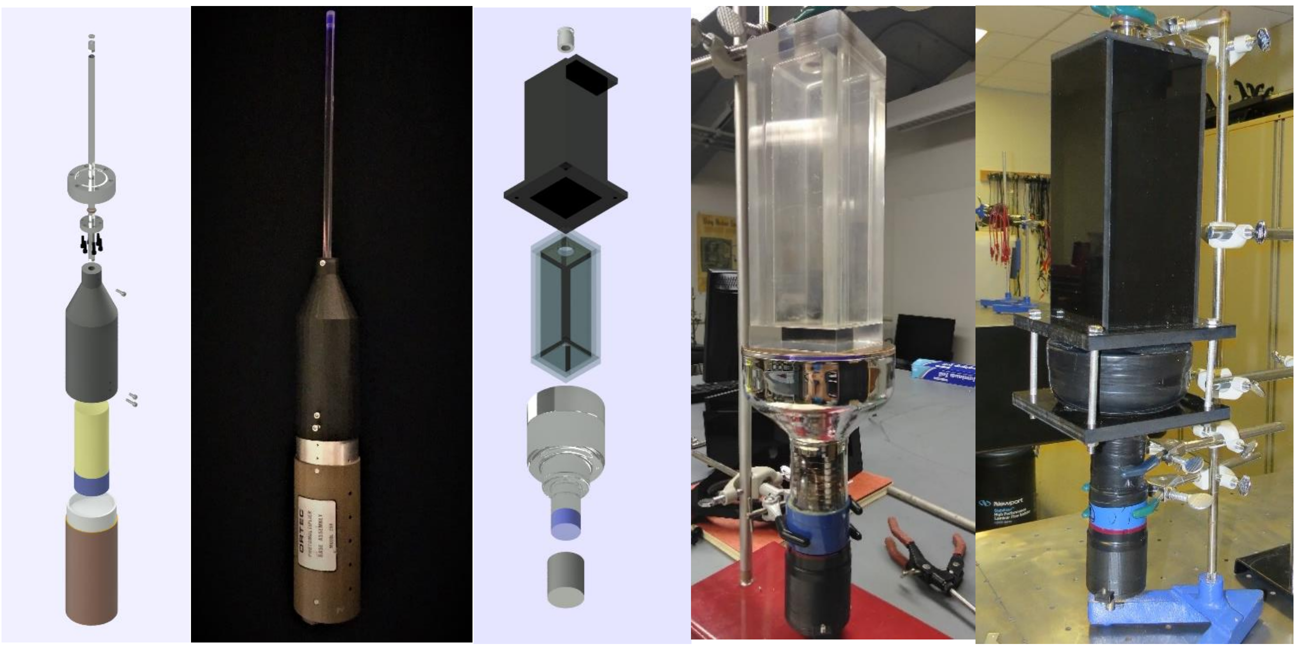

(a) (b) (c) (d) (e)

Figure 13. The getter detector and the turbopump detector. (a) Exploded view of the getter detector. **(b)** Photograph of the getter detector without light-tight wrap. **(c)** Exploded view of the turbopump detector. **(d)** Photograph of the turbopump detector without the light-tight acrylic box. **(e)** Photograph of the light-tight turbopump detector.

VII. Future Work

Future work will proceed in two directions. First, the Exploding Wire Experiment needs to be planned, constructed and carried out. Most of the remaining work and unsolved problems involve the design of the exploding wire apparatus itself, which is being handled by James McLean and his team. For the Houghton team, which is responsible for the detectors and the test chamber, items 2-5 from the list below still need to be addressed. Realistically, the most likely time frame for this experiment to take place is mid-summer 2021.

The other future project is to plan and perform a second OMEGA ride-along experiment. The purpose of this experiment would be to test the results of the Geant4 simulations and the consequently required detector modifications.

The following items still need to be addressed, listed in order of urgency.

1. **Geant4 simulations.** Using the Geant4 simulation code, a more careful analysis of the contribution of various sources of background needs to be made. To do this will require the code to model additional components of the detector and the environment, and new decay modes – particularly the beta decay of the first excited state of ^{26}Al.

   It would also be beneficial for the code to be modified to handle the detector response in a more realistic way that would better account for light attenuation, triggering, scintillator crosstalk, linear gate bias and offset effects, and PMT noise. In addition to studying the background and shielding options, the simulation should be applied to the problem of absolute detector efficiency.

2. **Getter detector.** The light attenuation in the acrylic lightguide needs to be measured and compared to the attenuation of other light guide options. A new light guide and detector needs to be assembled that transmits more of the scintillation light.

3. **Turbopump detector.** Low-pass filters and revised signal processing electronics need to be tested as a means to address the individual photon pulses from the 9823KB PMT with low intensity light resulting from the long decay time. If these are unsuccessful, the B133D01 PMT should be reinstated.

4. **Electronics.** Even if it is not required in order to use the 9823KB phototube, it would be advisable to look at designing a new signal processing and acquisition system. The current system is mostly limited by the use of two 1970s-era EG&G LG 105/N linear gates. There are two options:

   a. Replace the LG 105/N linear gates but continue to use NIM electronics for separating the fast and slow components to read into the FemtoDAQ or other acquisition system, such as a Caen DT5781 Quad Digital MCA. Using different linear gates would allow us to separately filter the fast and slow components, as well as reduce the dead time by about a factor of 5.

   b. Another option, made possible by the fact that Houghton just started a program in electrical engineering and hired three electrical engineers, would be to develop our own FPGA-based acquisition system that could be programmed to process everything right within the FPGA itself without the need for NIM electronics or even much post-processing analysis. This could form the basis of several EE student projects and a collaboration with one of the EE professors. In the end, this would allow the ultimate in noise reduction and signal separation.

5. **Valves.** In order to carry out the Exploding Wire Experiments, pneumatic valves need to be inserted between the turbopump trap detector and pump to stop any backflow out of the trap after the shot, and also between the beamline and the test chamber to maintain the low pressure in the beamline after the wire explodes.

6. **New auxiliary controller.** Currently, an Arduino Mega is used to control turning on the high voltage to the PMT and connecting the signal cables after the shot. It would be advantageous if the Arduino could be programmed remotely over ethernet, since it is sometimes difficult for experimenters to have access to LeCave. This is nearly impossible with an Arduino. Moreover, for the Exploding Wire experiment it would be very helpful to have the microcontroller also control opening and closing the valves to the detectors and between the beamline and test chamber. For this reason, we are considering replacing the Arduino with a more powerful Raspberry Pi 4.

7. **Ion pump trap.** The third concept for trapping the gas containing the reaction products is to use an ion pump. For this reason a Gamma 45S ion pump configured as a triode was recently purchased, and should arrive some time

after we finish this summer. This pump will eventually need to be modified by widening the gap between the magnet poles to allow a 19 mm thick phoswich detector to be inserted. Also, the wall will need to be thinned or replaced to allow beta particles to reach the detector. Initially however, it could be tested with nuclei that release gamma rays able to penetrate the wall.

VIII. Presentations since summer 2019

Tyler Kowalewski, Salvatore Ferri, Steven Raymond, Mark Yuly, Stephen Padalino, Chad Forrest, Craig Sangster, and Sean Regan. "Inertial Confinement Fusion as a Tool to Study Fundamental Nuclear Science," National Ignition Facility (NIF) and Jupiter Laser Facility (JLF) User Groups Joint Meeting, Livermore, CA, February 3-5, 2020; 61st Annual Meeting of the APS Division of Plasma Physics, Fort Lauderdale, Florida, October 21-25, 2019.

This material is based upon work supported by the Department of Energy [National Nuclear Security Administration] University of Rochester "National Inertial Confinement Program" under Award Number(s) DE-NA0004144.

---

[1] J. Melendez and I. Ramirez, Astrophys. J. **615**, L33 (2004); M. Asplund et al., Astrophys. J. **644**, 229 (2006); M. Kanga, Y. Hub, H. Hua and S. Zhub, Journal of Cosmology and Astroparticle Physics **2012**, 011 (2012).

[2] S.N. Abramovich, B.Ya. Guzhovskij, V.A. Zherebtsov, and A.G. Zvenigorodskij, International Nuclear Data Committee Report INDC(CCP)-326/L+F, (1991).

[3] A.J. Koning, S. Hilaire and M.C. Duijvestijn, "TALYS-1.0", Proceedings of the International Conference on Nuclear Data for Science and Technology, April 22-27, 2007, Nice, France, editors. O.Bersillon, F.Gunsing, E.Bauge, R.Jacqmin, and S.Leray, EDP Sciences, 2008, p. 211-214.

[4] S.N. Abramovich, B.Ya. Guzhovskij, V.A. Zherebtsov, and A.G. Zvenigorodskij, International Nuclear Data Committee Report INDC(CCP)-326/L+F, (1991).

[5] A.J. Koning, S. Hilaire and M.C. Duijvestijn, "TALYS-1.0", Proceedings of the International Conference on Nuclear Data for Science and Technology, April 22-27, 2007, Nice, France, editors. O.Bersillon, F.Gunsing, E.Bauge, R.Jacqmin, and S.Leray, EDP Sciences, 2008, p. 211-214.

[6] R.W. Kavanagh and C.A. Barnes, Phys. Rev. **112**, 503 (1958).

[7] N.A. Bostrom,E.L. Hudspeth, and I.L. Morgan, Phys. Rev. **105**, 1545 (1957).

[8] M. Yuly, S Padalino, M. Coates and K. Cook. "A possible measurement of the ^{3}H(t,γ)^{6}He cross section at low energy" in Nuclear and Plasma Diagnostics for the EP-OMEGA and MTW Laser Systems, Proposal Submitted to the Laboratory for Laser Energetics #416231G, (2016).

[9] M. Yuly, S Padalino, M. Coates and K. Cook. "A Phoswich Detector System to Measure the ^{3}H(t,γ)^{6}He Cross Section using ICF" in Nuclear and Plasma Diagnostics for the EP-OMEGA and MTW Laser Systems, Proposal Submitted to the Laboratory for Laser Energetics #416231G, (2017).

[10] Mark Yuly, Stephen Padalino, Emma Bruce, Katelyn Cook, and Sarah Hull. "Measuring Low Energy Nuclear Cross Sections using ICF" in Nuclear and Plasma Diagnostics for the EP-OMEGA and MTW Laser Systems, Proposal Submitted to the Laboratory for Laser Energetics #416231G, (2018).

[11] Mark Yuly, Stephen Padalino, Tyler Kowalewski, Salvatore Ferri and Steven Raymond. "Inertial Confinement Fusion as a Tool to Study Fundamental Nuclear Science, The rapid isotope-counting system (RICS) using a hollow box phoswich detector" in Nuclear and Plasma Diagnostics for the EP-OMEGA and MTW Laser Systems, Proposal Submitted to the Laboratory for Laser Energetics #416231G, (2019).
[12] R. E. Azuma, E. Uberseder, E. C. Simpson, C. R. Brune, H. Costantini, R. J. de Boer, J. Gorres, M. Heil, P. J. LeBlanc, C. Ugalde, and M. Wiescher. Phys. Rev. C **81**, 045805 (2010).
[13] G.M. Hale and D. C. Dodder, Proceedings of the International Conference on Nuclear Cross Sections for Technology, NBS Special Publication 594 (1979) (Los Alamos Report LA-UR-79-2896).
[14] D. B. Sayre et al. Phys. Rev. Lett. **111**, 052501 (2013).
[15] C. R. Brune et al. Phys. Rev. C **92**, 014003 (2015).
[16] R. K. Smither and L. R. Greenwood, Journal of Nuclear Materials **123**, 1071-1077 (1984); M. Sasao et al., Phys. Rev. C **35**, 2327 (1987); T. Nakamura et al., Phys. Rev. C **43**, 1831 (1991); A. Pavlik et al., Phys. Rev. C **57**, 2416 (1998).
[17] National Nuclear Data Center, information extracted from the NuDat 2 database, http://www.nndc.bnl.gov/nudat2/.
[18] S. Agostinelli et al., Nucl. Instrum. Methods **506**, 250-303 (2003); J. Allison et al., IEEE Trans. Nucl. Sci. **53**, 270-278 (2006); J. Allison et al., Nucl. Instrum. Methods **835**, 186-225 (2016).
[19] Rene Brun and Fons Rademakers, Proceedings AIHENP'96 Workshop, Lausanne, Sep. 1996, Nucl. Inst. & Meth. in Phys. Res. A **389,** 81-86 (1997).